# Cavity cooling of translational and ro-vibrational motion of molecules: *ab initio*-based simulations for OH and NO

**Markus Kowalewski**[1], **Giovanna Morigi**[2], **Pepijn W. H. Pinkse**[3], **Regina de Vivie-Riedle**[1]

[1] Departement of Chemistry, Ludwig-Maximilian-Universität München, Butenandt-Str. 11, D-81377 München, Germany, fax: +49-89-218077133, e-mail: Regina.de_Vivie@cup.uni-muenchen.de
[2] Departament de Fisica, Universitat Autonoma de Barcelona, E-08193 Bellaterra (Barcelona), Spain
[3] Max-Planck-Institut für Quantenoptik, Hans-Kopfermann-Str. 1, D-85748 Garching, Germany

Submitted 03.08.2007

**Abstract** We present detailed calculations at the basis of our recent proposal for simultaneous cooling the rotational, vibrational and external molecular degrees of freedom [1]. In this method, the molecular rovibronic states are coupled by an intense laser and an optical cavity via coherent Raman processes enhanced by the strong coupling with the cavity modes. For a prototype system, OH, we showed that the translational motion is cooled to few $\mu$K and the molecule is brought to the internal ground state in about a second. Here, we investigate numerically the dependence of the cooling scheme on the molecular polarizability, selecting NO as a second example. Furthermore, we demonstrate the general applicability of the proposed cooling scheme to initially vibrationally and rotationally hot molecular systems.

**PACS** 33.80.Ps, 32.80.Lg, 42.50.Pq

## 1 Introduction

Control at the quantum level over both the internal and external degrees of freedom of gas-phase molecules has been pursued by several groups worldwide [2]. This intense activity has various ultimate goals, such as the realization of Bose-Einstein condensation of complex systems, the emergence of new ultracold chemistry [3], and the applications for high-precision measurements [4,5] and quantum information processing [6,7,8]. The efficient preparation of molecules into predetermined quantum states is the prerequisite for control. Various approaches are currently applied. Established methods for generating ultracold alkali dimers use photoassociation and, or in combination with, Feshbach resonances [9]. Another approach is based on buffer gas cooling, in which the molecules are thermalized with a cold buffer gas [10]. Decelleration of molecules from supersonic nozzles [11, 12], filtering from an effusive source [13] and collisional techniques [14,15] are other methods which have been developed to produce samples of cold molecules.

The application of laser cooling techniques, which had tremendous impact on atomic and optical physics [16, 17,18], to molecules turned out to be inefficient so far. Here, multiple scattering channels, due to the molecular ro-vibrational structure, are coupled by spontaneous emission, leading to uncontrolled heating of the system as an undesired side effect. Even when heating can be suppressed, the resulting cooling time is long and may only be feasible for molecules which are confined in external traps for very long times [19,20]. Proposals aimed at overcoming this problem have been suggested: Sophisticated laser-cooling schemes, based on optical pumping the ro-vibrational states [21,22] and optimally modulated femtosecond excitation pulses [23,24], achieve efficiencies which are still severely limited by spontaneous decay and its inherent long time duration.

An alternative way to optically cooling external degrees of freedom of molecules was proposed and studied in [25,26,27,28], and it makes use of the enhancement of stimulated photon emission into the cavity mode over the spontaneous decay. This mechanism was successfully applied for cooling the motion of atoms [29,30,31]. In a recent work [1], we extended this idea and proposed to optically cool the external as well as the *internal* molecular degrees of freedom by using the coupling to a cavity. In the proposal the molecules are cooled by a Raman process in which photons from an intense laser are scattered into the modes of a resonator by molecular dipole transition, thereby cooling the motion to the cavity linewidth and the ro-vibrational degrees of freedom to the ground state. The dynamics is numerically simulated for the OH radical as a prototype system and for a realistic set of experimental parameters, while the molecular properties are calculated with state-of-the-art ab initio calculations. Starting with an internal temperature of 300 K we could show that the translational motion is

cooled to a few $\mu$K and the internal state is cooled to its ro-vibrational ground state [1].

In this article we provide the details of the theory and of the *ab initio* results at the basis of [1]. In order to demonstrate explicitly the general applicability of the proposed scheme, we present further numerical simulations where we apply it for the simultaneous cooling of vibrational and rotational degrees of freedom for OH in a set up with an artificial high temperature, such that several vibrational states are initially occupied. Moreover, we simulate cooling of a similar diatomic system, NO, whose $\pi$ bonding allows for a larger electronic polarizability.

This paper is structured as follows. First the central idea is introduced in section 2, followed by a detailed account of the theoretical model including the basic equations in section 3. In section 4 the two selected molecules OH and NO are introduced and their properties are evaluated with *ab initio* methods. In section 5 the experimental boundary conditions are given which are the final ingredients leading to the results presented in section 6. The paper closes with a summary, conclusions and outlook.

## 2 Optically cooling molecules to the ground state

The cooling method we propose is based on the enhancement of the (anti-Stokes) Raman transitions, where photons of an intense laser field are scattered by a molecular dipole transition into the modes of a cavity thereby cooling the external and the internal molecular motion, as sketched in Fig. 1. Spontaneous emission is largely suppressed, since the laser light is far detuned from all direct electronic transitions. The enhancement of coherent scattering into the cavity modes is obtained by

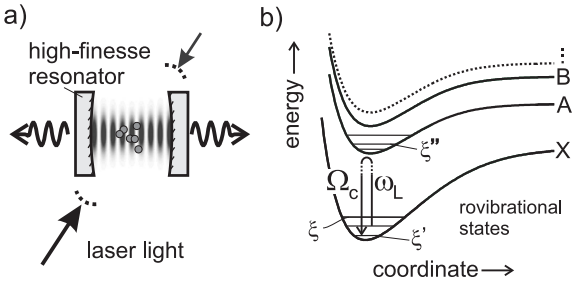


**Fig. 1** The idea in a nutshell: (a) molecules which are assumed to be confined in a high-finesse cavity interact with strong CW laser light. The laser intensity might be enhanced by a build-up cavity. (b) The laser light is far detuned from all direct electronic transitions from the ground state X to electronically excited states A,B,... in the molecules.The ro-vibrational energy of the molecules is reduced by a sequence of Raman transition, where laser photons are scattered into the cavity modes.

driving the Raman anti-Stokes transitions on resonance. For this purpose, the laser frequency is varied sequentially, in order to shift the comb of cavity resonances across the molecular anti-Stokes transitions, as sketched in Fig. 2. The external motion is initially cooled to the cavity linewidth by setting the laser frequency on the red-side of the Rayleigh line [32] in Fig. 2. In our numerical simulations we checked that this is a relatively fast stage, in which the internal motion is not affected by the scattering processes. Then, the ro-vibrational degrees of freedom are cooled as the laser frequency is sequentially tuned to address all relevant anti-Stokes lines. The ro-vibrational levels are hence sequentially emptied, till the molecules finally end up in their ground state.

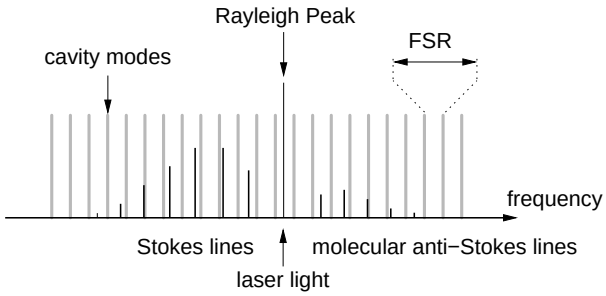


**Fig. 2** Combined with the cavity modes, the laser drives a sequence of coherent Raman anti-Stokes transitions which on average reduces the ro-vibrational energy of the molecules. The spectrum can be shifted relative to the fixed cavity lines by tuning the laser frequency. The frequency comb of the cavity modes is much denser than in the figure.

## 3 Model and basic equations

We now summarize the theoretical model, describing the quantum dynamics of the molecular internal degrees of freedom and of the modes of the cavity field. We consider a gas of molecules of mass $M$, prepared in the electronic ground state $X$, and with dipole transitions $X \rightarrow E$. Here, $E = \{A, ...\}$ is a set of electronically excited states, which may contribute significantly to the total polarizability. We denote by $|\xi\rangle$, $|\xi'\rangle$ the ro-vibrational states of the electronic ground state, such that the state $|X, \xi\rangle$ is at frequency $\omega_\xi^{(X)}$, and by $|\xi''\rangle$ the ro-vibrational states of the electronic excited states, with $|E, \xi''\rangle$ at frequency $\omega_{\xi''}^{(E)}$. The elements of the dipole moment $\mathbf{d}$ are

$$\mathcal{D}_{\xi\rightarrow\xi''} = \langle E, \xi''|\mathbf{d}|X, \xi\rangle. \quad (1)$$

Denoting by $\mathbf{p}$, $\mathbf{x}$ the conjugate momentum and position of the center of mass, the Hamiltonian describing the dynamics of the uncoupled molecular degrees of freedom

reads

$$H_{\rm mol} = \frac{\mathbf{p}^2}{2M} + \sum_{\xi} \hbar\omega_{\xi}^{(X)} |X,\xi\rangle\langle X,\xi| + \sum_{E,\xi''} \hbar\omega_{\xi''}^{(E)} |E,\xi''\rangle\langle E,\xi''|. \quad (2)$$

The transitions between molecular levels are driven by a far-off resonant laser and interact with an optical resonator as illustrated in Fig. 1a), undergoing a coherent dynamics which is described by the total Hamiltonian $H = H_{\rm mol} + H_c + V_c + V_L$. Here,

$$H_{\rm c} = \sum_{c} \hbar\Omega_c a_c^\dagger a_c \quad (3)$$

is the Hamiltonian for the cavity modes, where $a_c$ ($a_c^\dagger$) denotes the annihilation (creation) of a photon with energy $\hbar\Omega_c$, with wave vector $\mathbf{k_c}$, polarization $\epsilon_0$ and the (vacuum) electric field amplitude $\mathcal{E}_c$. The coupling between cavity modes and molecular dipole transitions is described by the term

$$V_{\rm c} = \sum_{c,\xi',E,\xi''} \hbar g_{c,\xi'\to\xi''}(z)\hat{a}_c \left(\hat{\sigma}^{E\dagger}_{\xi',\xi''} + \hat{\sigma}^{E}_{\xi',\xi''}\right) + \text{h.c.}, \quad (4)$$

where $g_{c,\xi'\to\xi''}(z) = \mathcal{E}_c(z)(\epsilon_0 \cdot \mathcal{D}_{\xi'\to\xi''})/\hbar$ is the vacuum Rabi coupling, whose dependence on the position along the cavity $z$ axis is determined by the corresponding spatial mode function, and

$$\hat{\sigma}^{E}_{\xi,\xi''} = |X,\xi\rangle\langle E,\xi''|, \quad \hat{\sigma}^{E\dagger}_{\xi,\xi''} = |E,\xi''\rangle\langle X,\xi| \quad (5)$$

are the corresponding dipole lowering and rising operators. The molecules are pumped by a laser, which couples to the dipole and is described by a classical field with amplitude $\mathcal{E}_L$, polarization $\epsilon_L$, frequency $\omega_L$, and wave vector $\mathbf{k_L}$. The laser is assumed to propagate perpendicular to the cavity axis, and the Hamiltonian term describing the coupling with the dipole takes the form

$$V_L = \sum_{\xi,E,\xi''} \hbar\Omega_{L,\xi\to\xi''} \mathrm{e}^{-\mathrm{i}(\omega_L t - \mathbf{k_L}\cdot\mathbf{x})} \left(\hat{\sigma}^{E\dagger}_{\xi,\xi''} + \hat{\sigma}^{E}_{\xi,\xi''}\right) + \text{h.c.}, \quad (6)$$

where $\Omega_{L,\xi\to\xi''} = \mathcal{E}_L(\mathcal{D}_{\xi\to\xi''}\cdot\epsilon_L)/\hbar$ gives the corresponding coupling strength. In the interaction Hamiltonian $V_L$, we keep the counterrotating terms, as we will consider parameter regimes where the rotating wave approximation is not valid.

Finally, cavity modes and dipole transitions couple to the modes of the electromagnetic field external to the resonator. We denote by $\Gamma_{\xi''\to\xi'}$ the decay rate along the dipolar transition $|E,\xi''\rangle \to |X,\xi'\rangle$, such that the linewidth of the state $|E,\xi''\rangle$ is $\Gamma_{\xi''} = \sum_{\xi'} \Gamma_{\xi''\to\xi'}$. The linewidth of the resonator modes is $2\kappa$, and we assume the regime in which the Free Spectral Range (FSR) $\Omega_{c+1} - \Omega_c \gg 2\kappa$.

We assume that the laser and the cavity modes are far-off resonance from the molecular transitions, as depicted in Fig. 1b), such that the most relevant processes are Raman transitions, i.e., incoherent Raman scattering in which a laser photon is absorbed and then emitted spontaneously, and coherent Raman scattering in which a laser photon is scattered into one cavity mode. The rate of spontaneous Raman scattering reads

$$\Gamma^{\gamma}_{\xi\to\xi'}(\mathbf{p}) = \sum_{E,\xi''} \Gamma_{\xi''\to\xi'} \left(\gamma^{+}_{E,\xi\to\xi''}(\mathbf{p}) + \gamma^{-}_{E,\xi\to\xi''}(\mathbf{p})\right) \quad (7)$$

and it depends on the molecular momentum $\mathbf{p}$ through the Doppler effect as

$$\gamma^{+}_{E,\xi\to\xi''}(\mathbf{p}) = \frac{\Omega^2_{L,\xi\to\xi''}}{(\Delta^{E}_{\xi,\xi''} + \mathbf{k_L}\cdot\mathbf{p}/M)^2 + \Gamma^2_{\xi''}/4} \quad (8)$$

$$\gamma^{-}_{E,\xi\to\xi''}(\mathbf{p}) = \frac{\Omega^2_{L,\xi\to\xi''}}{(\Delta^{E}_{\xi,\xi''} - 2\omega_L - \mathbf{k_L}\cdot\mathbf{p}/M)^2 + \Gamma^2_{\xi''}/4} \quad (9)$$

where $\Delta^{E}_{\xi,\xi''} = \omega^{(X)}_{\xi} - \omega^{(E)}_{\xi''} + \omega_L$ denotes the detuning between laser and internal transition. The rate $\Gamma^{\kappa}_{\xi\to\xi'}(\mathbf{p})$ gives the scattering rate of a photon from the laser into the cavity mode and its subsequent loss from the cavity.

To evaluate the rate of photon scattering into the cavity modes, we consider a standing wave cavity, and focus onto the regime in which the cavity photon is not reabsorbed by the molecules but lost via cavity decay [26]. Moreover, we assume that the molecular kinetic energy exceeds the height of the cavity potential. In this regime, we decompose the coupling constant $g_{c,\xi'\to\xi''}(z)$ into the Fourier components $g^{\pm}_{c,\xi'\to\xi''}$ at cavity-mode wave vector $\pm|\mathbf{k_c}|$, and write the rate of photon scattering into the cavity as $\Gamma^{\kappa}_{\xi\to\xi'}(\mathbf{p}) = \Gamma^{\kappa,+}_{\xi\to\xi'}(\mathbf{p}) + \Gamma^{\kappa,-}_{\xi\to\xi'}(\mathbf{p})$, where the sign $\pm$ gives the direction of emission along the cavity axis and

$$\Gamma^{\kappa,\pm}_{\xi\to\xi'}(\mathbf{p}) = 2\kappa \sum_{c,E,\xi''} \left|g^{\pm}_{c,\xi''\to\xi'}\right|^2 \left(\frac{\gamma^{+}_{E,\xi\to\xi''}(\mathbf{p})}{\left(\delta\omega^{+} \pm \mathbf{k_c}\cdot\mathbf{p}/M\right)^2 + \kappa^2} + \frac{\gamma^{-}_{E,\xi\to\xi''}(\mathbf{p})}{\left(\delta\omega^{-} \pm \mathbf{k_c}\cdot\mathbf{p}/M\right)^2 + \kappa^2}\right), \quad (10)$$

where $\delta\omega^{\pm} = \omega^{(X)}_{\xi} - \omega^{(X)}_{\xi'} \pm \omega_L - \Omega_c$ is the frequency difference between initial and final (internal and cavity) states. We note that the reabsorption and spontaneous emission of the cavity photon can be neglected when

$$\kappa \gg |g_{c,\xi'\to\xi''}\Omega_{L,\xi\to\xi''}/\Delta^{E}_{\xi,\xi''}|. \quad (11)$$

The basic condition for cavity cooling is that the rate of photon scattering into the cavity exceeds the corresponding spontaneous Raman scattering rate,

$$\Gamma^{\kappa}_{\xi\to\xi'}(\mathbf{p}) \gg \Gamma^{\gamma}_{\xi\to\xi'}(\mathbf{p}). \quad (12)$$

This is the regime on which we will focus.

*3.1 Rate equations*

We can now write the equations describing the damped dynamics of the molecules. For this purpose, we denote by $\mathcal{W}_\xi(p)$ the occupation of the molecular state $|X,\xi\rangle$ at momentum $p$.

An equation for the kinetic energy can be simply derived in the semiclassical limit. Let us first define by $\Delta p^2/2M$ the average change in kinetic energy in an infinitesimal interval of time $\Delta t$. This is given by $\Delta p^2/2M = \sum_\xi \Delta p_\xi^2/2M$, where

$$\Delta p_\xi^2 = \Delta t \int \mathrm{d}p \sum_{\xi',j=\pm} \Big[(p+j\hbar k)^2 \Gamma^j_{\xi'\to\xi}(p)\mathcal{W}_{\xi'}(p) - p^2\Gamma^j_{\xi\to\xi'}(p)\mathcal{W}_\xi(p)\Big] \tag{13}$$

and we have introduced, for convenience, the total rate $\Gamma^\pm_{\xi'\to\xi}(p) = \Gamma^{\kappa,\pm}_{\xi'\to\xi}(p) + \Gamma^\gamma_{\xi'\to\xi}(p)/2$. In the regime where the laser is tuned such that only Rayleigh scattering into the cavity mode is enhanced, the relevant processes will not change the internal state of the molecule. In this regime, when the rate of spontaneous Raman scattering is much smaller than the coherent cavity scattering one obtains the typical dynamics of Doppler cooling, see [33] for a detailed treatment. Here, the cooling rate is given by $(\hbar^2k^2/2M)\Gamma'(0)$, where $\Gamma'(0) \approx \sum_\xi \Gamma^j_{\xi\to\xi}(0)$ and the asymptotic value of the kinetic energy is

$$E^\infty_{\mathrm{kin}} = \frac{\hbar}{4}\frac{(\omega_L-\Omega_c)^2+\kappa^2}{|\omega_L-\Omega_c|}, \tag{14}$$

which is minimum for $\omega_L - \Omega_c = -\kappa$ and takes the value $E^{\infty,\min}_{\mathrm{kin}} = \hbar\kappa/2$ [32].

The generic rate equation, describing the dynamics of the population of the molecular state $\mathcal{P}_\xi = \int dp \mathcal{W}_\xi(p)$ reads

$$\dot{\mathcal{P}}_\xi = -\int dp \sum_{\xi'} \Big(\Gamma^\kappa_{\xi\to\xi'}(p) + \Gamma^\gamma_{\xi\to\xi'}(p)\Big)\mathcal{W}_\xi(p) + \int dp \sum_{\xi'} \Big(\Gamma^\kappa_{\xi'\to\xi}(p) + \Gamma^\gamma_{\xi'\to\xi}(p)\Big)\mathcal{W}_{\xi'}(p), \tag{15}$$

which requires the knowledge of all rates and populations at each instant of time. Assuming that the molecules have been previously cavity cooled to the cavity linewidth, and that the momentum distribution is not significantly modified by the inelastic processes that change the internal state of the molecule, then the rate of inelastic processes is

$$\int dp \Gamma^{\kappa,\pm}_{\xi\to\xi'}(p)\mathcal{W}_\xi(p) \approx \Gamma^{\kappa,\pm}_{\xi\to\xi'}(0)\mathcal{P}_\xi. \tag{16}$$

Hence, in this regime, the incoherent dynamics can be described by the rate equation

$$\dot{\mathcal{P}}_\xi = -\sum_{\xi'}\Big(\Gamma^\kappa_{\xi\to\xi'} + \Gamma^\gamma_{\xi\to\xi'}\Big)\mathcal{P}_\xi + \sum_{\xi'}\Big(\Gamma^\kappa_{\xi'\to\xi} + \Gamma^\gamma_{\xi'\to\xi}\Big)\mathcal{P}_{\xi'}, \tag{17}$$

whose stationary solution is found using the detailed balance principle.

The simulation of the cooling procedure uses rate equations for the molecular levels with the rates (7) and (10) as evaluated in the previous section. The sequence for the laser driven transitions is simulated by changing the detuning at the different steps. The cooling of the external degrees of freedom is the preliminary step. We have evaluated the cooling rate for the external motion with the laser frequency set to $\omega_L = \Omega_c - \kappa/2$, and checked that the internal molecular level distribution is practically unaffected during the cooling time. In the step for cooling the internal degrees of freedom, we then assumed that the motion was cooled at the Doppler limit, and set $p = 0$ in the rates (7) and (10). In the next section we report the details of the numerical treatment, for determining the parameters which give us the rates.

## 4 The molecular systems: OH and NO

We simulate the cooling scheme for OH and NO radicals. Cold ensembles of these two molecules are experimentally available [14,34,35,36]. We first apply the cooling scheme for an internal temperature of 300 K. Since at this temperature OH molecules are in the vibrational ground state, we also simulate the process for OH in a situation in which initially the internal temperature is artificially high, in order to investigate cooling of vibrational motion explicitly.

OH and NO can be modeled accurately by *ab initio* quantum chemistry methods. They have a similar electronic valence structure which allows to compare their electronic properties. In particular, the unpaired electron leads to a significant spin orbit splitting of $139\,\mathrm{cm}^{-1}$ and $123\,\mathrm{cm}^{-1}$ for the $X^2\Pi$ ground states of OH and NO, respectively. $\Lambda$-doubling occurs due to the coupling between rotation and electronic angular momentum. The doubling lies in the MHz regime and is different for the $X^2\Pi_{3/2}$ and the $X^2\Pi_{1/2}$ components. We only consider one $\Lambda$-state, since states of different parities are not coupled by Raman transitions. The hyperfine splittings in OH, due to the nuclear spin of the hydrogen atom, are neglected since angular momentum conservation for the rotational Raman transitions inhibits transitions between these sublevels. Hence, we assume that it is possible to prepare the molecules in the lower lying $X^2\Pi_{3/2}$ state for OH and $X^2\Pi_{1/2}$ for NO. With these assumptions we choose $J$ as the rotational quantum number.

Because of the Raman selection rule $\Delta J = 0, \pm 2$, matrix elements between rotational states with even and odd $J$ values vanish. This leads to two separate ladders for the scattering process with ground states $|X, v = 0, J = 0\rangle$ and $|X, v = 0, J = 1\rangle$, respectively.

The energy of the rotational levels reads

$$E_J = B(v)J(J+1) - D_j J^2(J+1)^2, \tag{18}$$

with

$$B(v) = B_e + B_{e,x1}(v + \frac{1}{2}) + B_{e,x2}(v + \frac{1}{2})^2. \tag{19}$$

The constants, including the anharmonicities, are taken from Ref. [37]. In particular, for OH they read$(B_e, B_{e,x1}, B_{e,x2}, \omega_e) = (18.871, \text{-}0.714, 0.0035, 3735.21)\,\text{cm}^{-1}$ while for NO they are $(B_e, B_{e,x1}, B_{e,x2}, \omega_e) = (1.7042, \text{-}0.01728, 0.000037, 1904.2)\,\text{cm}^{-1}$. The anharmonicity in the vibrational ladder is included in the *ab initio* potential energy surfaces (PES).

### *4.1 Molecular polarizabilities*

We now determine the molecular rotational and vibrational structure in order to evaluate the scattering rates for simulating the cooling dynamics. A relevant quantity is the polarizability $\alpha$, which is defined for molecular systems as

$$\boldsymbol{\alpha} = \sum_{E,\xi''} \frac{\mathcal{D}_{\xi\to\xi''}\mathcal{D}_{\xi''\to\xi}}{\hbar\Delta^E_{\xi,\xi''}} + \frac{\mathcal{D}_{\xi\to\xi''}\mathcal{D}_{\xi''\to\xi}}{\hbar(\Delta^E_{\xi,\xi''} - 2\omega_L)}, \tag{20}$$

and is expressed as a function of the laser frequency $\omega_L$ and the internal nuclear coordinates. Note that also higer lying excited states can have significant contributions. The polarizability is described as a tensor which can be expressed in terms of irreducible components. The isotropic part $\alpha^{(0)}$, defined as

$$\alpha^{(0)} = \frac{1}{3}Tr(\boldsymbol{\alpha}), \tag{21}$$

is responsible for transitions which do not change the angular momentum of the molecule. The traceless component $\alpha^{(2)}_{zz}$ along the main axis of the molecule, can be evaluated from

$$\alpha^{(2)}_{ij} = \alpha^{(2)}_{ji} = \frac{1}{2}\left(\alpha_{ij} + \alpha_{ji}\right) - \alpha^{(0)}. \tag{22}$$

This component is needed to describe ro-vibrational transitions associated with a change in $J$. In all subsequent formulas $\alpha$ represents the appropriate component. This general formulation allows us to treat all possible transitions between the internal states.

The transitions between the vibrational states can be written as the matrix element

$$\alpha_{v\to v'} = \langle \xi_v | \alpha(R) | \xi_{v'} \rangle, \tag{23}$$

in which the integration is over the nuclear coordinates $R$ and where $\xi_v$ indicates the pure vibrational states. The transition strength between the rotational levels is evaluated using the Placzek-Teller coefficients [38,39] for general diatomic molecules (shown in Tab. 1). The Placzek-Teller coefficient $S_{J\to J'}$ for the corresponding transition is multiplied with the square of the absolute value of the polarizability, giving the complete transition matrix element

$$|\alpha_{v,J\to v',J'}|^2 = |\alpha_{v\to v'}|^2 \cdot S_{J\to J'}. \tag{24}$$

The obtained value for $\alpha$ can be inserted in Eq. 7 and Eq. 10 to calculate the transition rates in the molecular system.

**Table 1** Placzek-Teller coefficients $S$ adapted to diatomic molecules. With the different cases for $J$ one can calculate Stokes and anti-Stokes transitions as well as Rayleigh scattering.

| $\Delta J$ | $S$ |
|---|---|
| $J$ | $\frac{[J(J+1)]^2}{J(J+1)(2J-1)(2J+3)}$ |
| $J+2$ | $\frac{3(J+1)^2(J+2)^2}{2(J+1)(J+2)(2J+1)(2J+3)}$ |
| $J-2$ | $\frac{3(J-1)^2J^2}{2(J-1)J(2J+1)(2J-1)}$ |

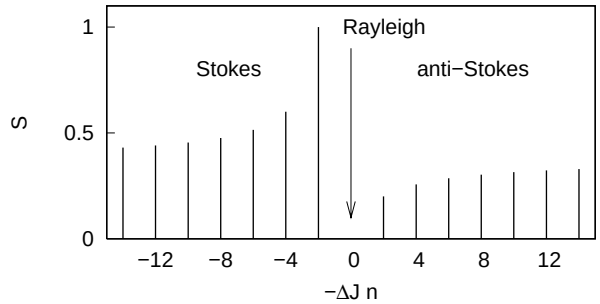


**Fig. 3** Illustration of the Placzek-Teller coefficients $S$ for the seven relevant Raman lines. The transitions indexed with $n$, which are allowed according to the selection rule $\Delta J = \pm 2$ are shown. For example, $-\Delta J n = 2$ refers to $J_{2\to 0}$ and $-\Delta J n = 4$ refers to $J_{3\to 1}$. The coefficients for the Rayleigh scattering $\Delta J = 0$ are not included in the picture.

### *4.2 ab initio calculations*

We carried out different types of *ab initio* calculations for all the relevant properties not directly available from

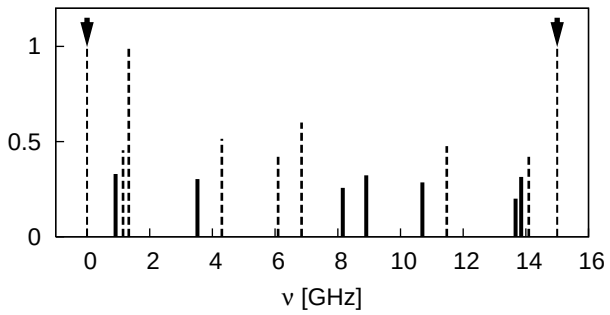


**Fig. 4** Reduced spectrum of the seven relevant Raman lines for OH. The Raman transitions are projected into one FSR. The solid lines indicate the driven anti-Stokes transitions. The dashed lines represent the corresponding Stokes lines in the Spectrum. The cavity resonances are the lines on left and on the right side highlighted by the arrows.

literature. The PES were obtained with Molpro [40] in a complete active space self consistent field (CASSCF) calculation and were further improved with a multi reference configuration interaction (MRCI) step. A valence triple zeta single atom basis set (cc-pVTZ) [41] was used. For the OH radical we chose an active space of 11 orbitals which includes all electrons except the 1s core orbital from the oxygen. The NO was treated in a similar way with 12 active orbitals and only leaving out the 1s core orbitals from the oxygen and the nitrogen atom.

For the calculation of the polarizability linear response theory on the same CASSCF [42,43] level were performed. This method is implemented in the program package DALTON [44]. The quality and convergence of the resulting polarizabilities were checked through several tests. The finite field method is used for comparison with the values in the static limit where $\omega_L = 0$. The static polarizability of a particle can expanded in a Taylor series with respect to the perturbation of an electric field, such that $\alpha$ is found from

$$\alpha^{FF} = \frac{\partial^2 E(\boldsymbol{\mathcal{E}})}{\partial \mathcal{E}_i \partial \mathcal{E}_j}. \tag{25}$$

The differentiation is done numerically with small field strengths. With this method several basis set checks (see Tab. 2) were performed for OH on the CASSCF level mentioned before. It turned out (as already mentioned in earlier publications [46]) that the results are very sensitive to the choice of the basis set. The addition of diffuse functions gives the better results. Higher angular momentum f-polarization functions have only a little effect on the polarizability. It turned out that correlation consistent basis sets (cc-pVXZ) [41,47] are more adequate for this task than the widely used 6-31G basis sets [48]. The aug-cc-pVTZ basis set was chosen for the polarizability calculations as a good compromise between size and quality of the result. This basis set was used to compare the result from the finite field calculations against linear response calculation in the static limit at zero frequency, where both methods should give equal results (Tab. 3). The obtained values differ less than 1 % and hence we can assume to have reasonable values. The calculated polarizability function in dependence of the OH bond length is shown in Fig. 5. The function has been calculated for a laser wavelength of 532 nm.

**Table 2** Single point polarizability calculations for OH with various basis sets. All calculations were carried out with on the CASSCF level of theory with the finite field method ($\mathcal{E} = 0.001$ au) at the equilibrium geometry. Listed are the needed tensor components $\alpha^{(0)}$ and $\alpha^{(2)}_{zz}$. Additionally the corresponding dipole moment is printed (The experimental value is $\mu_z = 0.657$ au= 1.67 Debye [45]). All values are given in atomic units.

| Basis set | $\alpha^{(0)}$ | $\alpha^{(2)}_{zz}$ | $\mu_z$ |
|---|---|---|---|
| 6-31G(d,p) | 3.809 | 2.172 | 0.711 |
| 6-31G++(d,p) | 4.936 | 1.652 | 0.741 |
| aug-cc-pVDZ | 6.826 | 1.438 | 0.648 |
| cc-pVTZ(d,p) | 5.194 | 1.836 | 0.667 |
| cc-pVTZ | 5.105 | 1.928 | 0.668 |
| aug-cc-pVTZ(d,p) | 7.230 | 1.188 | 0.648 |
| aug-cc-pVTZ | 7.240 | 1.200 | 0.645 |
| aug-cc-pVQZ | 7.407 | 1.069 | 0.646 |
| aug-cc-pVQZ(d,p) | 7.403 | 1.060 | 0.647 |

**Table 3** Comparison between the OH polarizabilities from the finite field and the linear response calculations at the CASSCF/aug-cc-pVTZ(d,p) level of theory. Additionally the dynamic polarizability at 532 nm is shown. All values are given in atomic units.

| Method | $\alpha^{(0)}$ | $\alpha^{(2)}_{zz}$ |
|---|---|---|
| Finite field | 7.23 | 1.19 |
| Linear response, static limit | 7.21 | 1.17 |
| Linear response, $\lambda = 532$ nm | 7.39 | 1.15 |

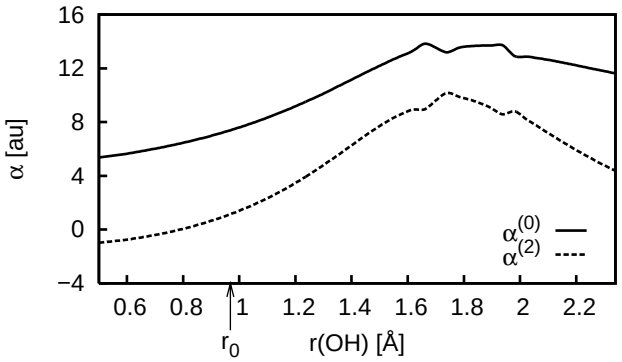


**Fig. 5** The polarizability function in dependence of the bond length for OH at a laser wavelength of 532 nm. The isotropic part $\alpha^{(0)}$ is used for the calculation of the Rayleigh scattering transitions. The traceless part $\alpha^{(2)}_{zz}$ of the tensor determines the rotational transitions. The equilibrium geometry is indicated by $r_0$. The wiggles between 1.6 Å and 2.0 Å are artifacts from resonances where the detuning $\Delta^E_{\xi,\xi''}$ is near zero. These singularities were smoothed by an interpolation.

Both curves for the isotropic and the traceless part show a typical increase with greater bond lengths reaching a maximum between 1.6 Å and 2.0 Å. In this area the $X^2\Pi$ and $A^2\Sigma^+$ state come closer (see Fig. 1) and their energy difference matches the laser frequency. Here, the Raman approximation [49] becomes invalid and the evaluated data points show a singularity. This effect is smoothed by an interpolation routine. The remaining wiggles have no effect on the results as they lie outside the nuclear range relevant in the considered Raman process.

The vibrational eigenvalues and eigenfunctions of the molecules were evaluated with a relaxation method using propagation in imaginary time with an additional diagonalization step [50]. This method is used to determine the vibrational wavefunctions in the ground state and first electronic excited state, necessary to obtain the relevant Franck-Condon factor of the system.

## 5 Experimental parameters

We now discuss the experimental parameters, which are required in order to implement efficiently the cooling scheme. We assume that the OH or NO molecules are prepared in the lower-lying component of the $X^2\Pi$ electronic ground state with a motional temperature around or slightly below 1 K. This could be realized with, e.g., helium-buffer-gas cooling [10], electrostatic filtering [13], or decelerator techniques [11,12]. However, as the purpose of this paper is to demonstrate in particular the cooling of the internal motion of the molecule, the filtering method [13] matches most closely our assumed initial conditions. At $T \approx 300\,\mathrm{K}$ only the first nine rotational levels of OH are occupied with a population $> 10^{-3}$. The first vibronic excitation for OH has an energy of $3727.95\,\mathrm{cm}^{-1}$ [37], and thus only the ground state $v = 0$ is occupied. For NO there are 25 rotational levels and because the vibronic excitation lies at $1904.2\,\mathrm{cm}^{-1}$ again only the ground state is occupied.

We choose a laser wavelength of 532 nm. Since this can be generated by frequency doubling of 1064 nm light, commercial systems are available with ample power, with high quality of the beam profile and which run at single frequency. The frequency of this light is far below that of the OH A-X ro-vibronic band. We assume to have single-frequency light of 10 W enhanced by a factor of 100 by a build-up cavity in a $\mathrm{TEM}_{00}$ mode, corresponding to a Rabi coupling $\Omega_{L,0\to0} = 2\pi \times 69\,\mathrm{GHz}$ and frequency $\omega_L = \omega_0^{(A)} - \omega_0^{(X)} - \Delta$ with $\Delta \approx 2\pi \times 407\,\mathrm{THz}$. Note that these intracavity intensities are routinely achieved in some commercial devices.

The laser frequency should be varied during cooling, in order to drive (quasi-)resonantly the cooling transitions. In combination with the broad spectrum of cavity modes, the laser only needs to be varied over one FSR to address all anti-Stokes lines. Fig. 4 displays the Stokes and anti-Stokes Raman lines as a function of the frequency modulus the FSR. Most commercial systems delivering high-power 532 nm light are not tunable, but this does not seem a fundamental problem. The build-up cavity will require tracking while the pump laser is scanned, which is also possible with today's technology.

We choose a high-finesse optical Fabry-Perot-type cavity with a length of $L = 1\,\mathrm{cm}$, which seems large enough to accommodate a trapping device as e.g., demonstrated in refs. [19,20,51,52]. This length leads to a free-spectral range (FSR) of $15 \times 2\pi\,\mathrm{GHz}$. For simplicity we assume that the cavity only supports zeroth-order transverse modes. The cavity half-linewidth is set to $\kappa = 75 \times 2\pi\,\mathrm{kHz}$, and the coupling $g_{c,0\to0} = 2\pi \times 116$ kHz. This is achieved with a mode volume of $3.2 \times 10^{-13}\,\mathrm{m}^3$, assuming a mode waist of $w_0 = 6\,\mu\mathrm{m}$, and a cavity finesse $F = 10^5$, i.e., a mirror reflectivity of 0.999969. In practice it might be necessary to choose a near-degenerate setup, e.g. a near-confocal cavity, in order to avoid higher-order cavity modes from appearing everywhere in the reduced spectrum, possibly coinciding with Stokes lines. Choosing such a degenerate setup actually increases the possibilities of scattering light into the cavity, increasing the cooling rate. There is one caveat: if the higher-order transverse cavity modes are not exactly degenerate with the zeroth order, this will lead to a cavity linewidth which will appear broadened and all lines in the reduced spectrum should be convoluted with this cavity linewidth. However, we do not expect this to be an issue, not even in a near-degenerate cavity, as our scheme is robust against a small number of coincidences between Stokes and anti-Stokes lines.

## 6 Cooling simulation results

### *6.1 Rotational cooling of OH and NO radicals*

We now simulate the cooling of OH and NO with the experimental parameters as described above. We start with the OH radical as the molecule of main interest. Fig. 6 and Fig. 8 show the results of the simulation. The FSR has been fine tuned so that the transitions $J_{3\to1}$ and $J_{2\to0}$ could be pumped simultaneously. In general, the spectral lines of a molecular system are not equally spaced and in general only one transition at a time can be addressed. However, two transitions can be selected simultaneously by tuning the FSR so that two cavity lines coincide with two transitions.

In Fig. 6 two different sequences are shown. The dashed curve represents a simple "top-down" variant which cools down the molecule to the ground states beginning from the highest occupied level. The solid curve is a manually optimized sequence in order to obtain a faster decrease of the expectation value $\langle J\rangle = \sum_J \mathcal{P}_J J$.

Snapshots of the population time evolution are shown in Fig. 7 and Fig. 8. In the top-down sequence, Fig. 7, we start driving the transitions corresponding to the

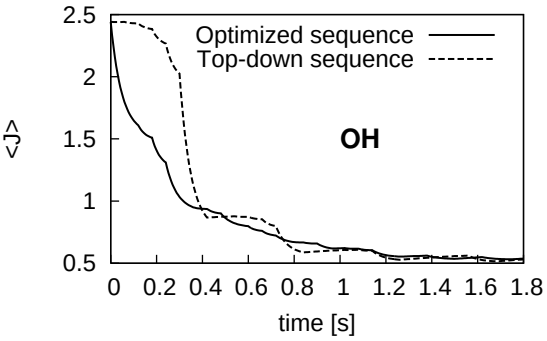


**Fig. 6** Rotational cooling of OH starting from 300 K. The expectation value $\langle J\rangle = \sum_J \mathcal{P}_J J$ of the rotational quantum number is plotted against time. The solid line shows a cooling process with a manually optimized laser sequence. The dashed line represents a "top-down" process where all higher levels are emptied sequentially in multiple cycles.

highest occupied states, $J_{8\to6}$ and $J_{7\to5}$, continuing with the subsequent anti-Stokes transitions. Every step lasts about 60 ms, whereby this optimal value was found empirically. After the first cycle 88 % of the population is in the states $J = 0, 1$. To achieve a lower final temperature the procedure is repeated six times. The rate for the decrease in $\langle J\rangle$ is 2.3 Hz. In the optimized sequence, first the $J = 2$ and $J = 3$ levels are addressed. In Fig. 8 this can be seen in the snapshot at 120 ms. Here a large population fraction is transferred to the two ground states. In the next step (after 240 ms) the transitions $J_{5\to3}$ and $J_{4\to2}$ are driven sequentially for 60 ms each. Repeating the first step, more than 90 % of the population is transferred to the ground states. By addressing the levels $J > 5$ and repeating the whole procedure, 98.8 % of the population is transferred to the two ground states $J = 0$ and $J = 1$ after 1680 ms. The achieved rate for the decrease in $\langle J\rangle$ is 3.6 Hz.

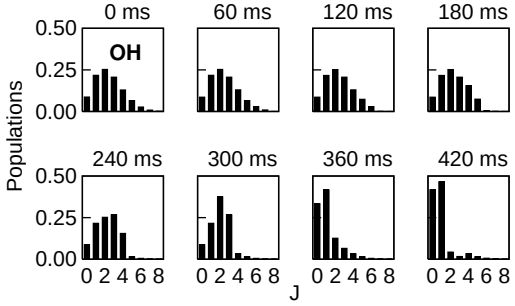


**Fig. 7** Populations at each step of the cooling process for the "top-down" sequence in the first cycle. Each transition is driven for 60 ms.

We also checked the effect of spontaneous Raman-processes on the vibrational state distribution when the rotational motion is cooled, and found only little vibrational heating. After a complete sequence of 1.8 s less than 1 % is in the state $v = 1$. Without cavity cooling, the rotations are heated, such that, the expectation value $\langle J\rangle$ rises from 2.44 to 2.56 on time scales of the order of 1.8 s.

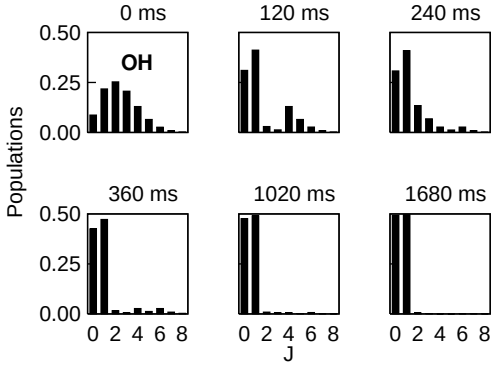


**Fig. 8** Populations at selected times of the cooling process for the manually optimized sequence. Each transition is driven for 60 ms.

To analyze the dependence of the cooling process on the related molecular properties, we now simulate cooling of a NO molecule, whose level structure in the electronic ground state is similar to the OH radical while the rotational and vibrational constants differ. In contrast to the more elaborate calculations of OH, the polarizability of NO was calculated in the quasi-static limit. This is a reasonable approximation as long as the ground state is coupled far-off resonance from the excited state. Due to the $\pi$-bonding in the NO radical the value for the polarizability is about 4 times greater than in the OH radical. Hence, compared to OH, NO offers a larger polarizability, which increases the cooling rate. On the other hand, due to the smaller rotational constant 25 rotational states are occupied at 300 K. Thus, NO is characterized by a broader distribution over the rotational levels than OH, which increases the cooling time. The result for the cooling procedure is shown in Fig. 9 and Fig. 10 for the manually-optimized sequence. It turned out that it is a good choice to start the sequence by addressing the levels near the maximum of the initial Boltzmann distribution (Fig. 10), in this case at levels $J = 12, 13$. Every transition is driven for 5 ms. After 60 ms the maximum of the distribution function is shifted to the ground-state levels $J = 0, 1$. The next step is started in the states $J = 20, 19$ and after 155 ms more than 50 % are in the two defined ground states. After 965 ms 99.2 % of the population is in the lowest two states. The optimal rate for the decrease in $\langle J\rangle$ is 5.3 Hz. In order to make a comparison with OH, we repeat the simulation for NO by taking the same initial internal distribution of only nine levels (which would correspond, in an experiment, to a sample of NO molecules at about 25 K). Due to the larger polarizability of NO, the cooling is about 12 times

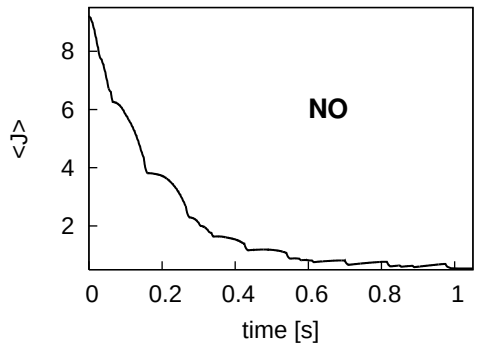


**Fig. 9** Rotational cooling of NO with an initial temperature of 300 K. The sequence for driving the transitions was manually optimized. Due to the larger polarizability the NO radical can be cooled faster than OH although more states are occupied.

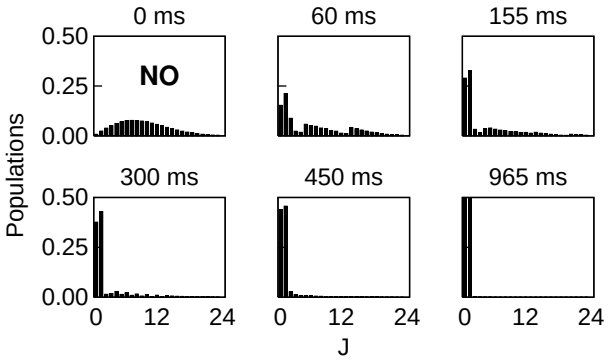


**Fig. 10** Populations during the cooling process for NO with an optimized sequence. The initial distribution corresponds to a temperature of 300 K. Various stages of the cooling process are shown.

faster than in the case of OH, and the optimal rate for the decrease in $\langle J \rangle$ is 43 Hz.

### *6.2 Cooling of the vibrational and rotational motion*

To test the efficiency of our scheme for cooling vibrational excitations, we consider again OH molecules and construct a scenario where the vibrational temperature is artifically high, taking an initial distribution in which the first nine *vibrational* levels are appreciably occupied. First we just cool the vibrational degrees of freedom, neglecting the Placzek-Teller coefficients. In this case, not only the absolute value of the polarizability, but also its finite slope with respect to the internuclear coordinate (see Fig.5) is important.

A roughly optimized frequency sequence for this procedure leads to the fast cooling process shown in Fig. 11, demonstrating that the concept works. However, it overestimates the cooling rate because the neglected Placzek-Teller coefficients for anti-Stokes transitions are smaller than 0.5.

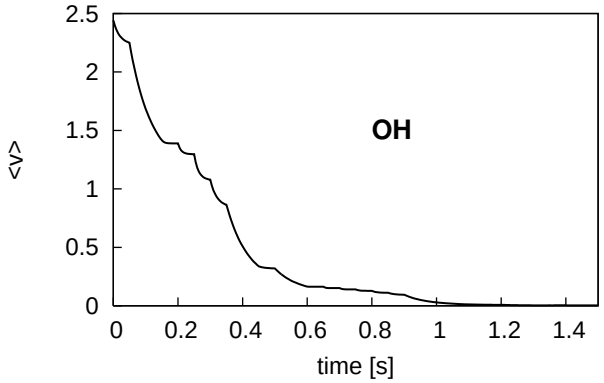


**Fig. 11** Cooling of the vibrational motion of OH for an initial thermal distribution where the first nine levels are significantly occupied.

In the next step the rotational degrees of freedom are combined with two vibrational levels each containing nine rotational substates. All initial population is in $v = 1$, with a 300 K rotational temperature. The task of achieving a good result for both $\langle v \rangle$ and $\langle J \rangle$ is now more complicated but still feasible. The roughly optimized sequence of Fig.12 is an example where vibrational and rotational degrees of freedom have been cooled simultaneously. For these results, the selection rules are exploited such as to reduce $\langle v \rangle$ and $\langle J \rangle$ simultaneously as much as possible. However, as can be seen in the figure, this is not always possible. In the beginning the transitions $v_{1\to0}J_{3\to1}$ and $v_{1\to0}J_{2\to0}$ are driven for 100 ms each. In the next step the transition $v_{1\to0}J_{1\to1}$ is driven. Here $\langle v \rangle$ still becomes smaller but $\langle J \rangle$ stays constant. In the following step after, 300 ms, a compromise was made. The state $v = 1, J = 0$ has to be emptied but the logical target state $v = 0, J = 0$ is not accessible because the Placzek-Teller coefficient for the $J_{0\to0}$ transition is zero.

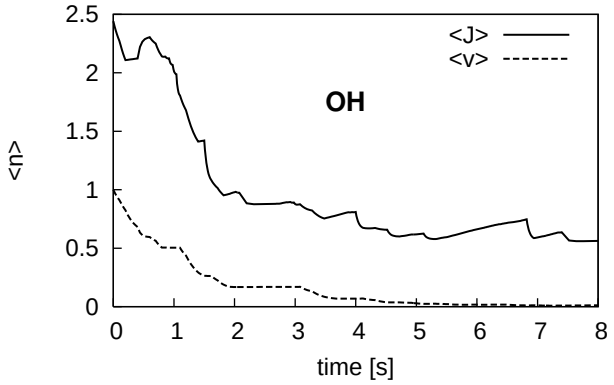


**Fig. 12** The expectation value of $n$ as function of time, where $n$ is a substitute for the quantum numbers $v$ and $J$, respectively. All population is initially in vibrational state $v = 1$ and the rotational levels follow a thermal distribution at 300 K.

Therefore the next accessible level, $v = 0, J = 2$, is used, which results in an increase in $\langle J \rangle$. Note that $J$ changes by 2 and $v$ by 1 and thus the variations in $\langle J \rangle$ are larger than those in $\langle v \rangle$. The further progression for the laser induced transitions implies the alternation of two principles: transferring populations to the lower vibrational states like for the first cooling steps and cooling the rotational levels without vibrational heating. It turned out that for the further cooling steps it is more effective to first cool the rotational motion without changing the vibrational motion before transferring the population to the vibrational ground state.

In the end of the procedure $\langle v \rangle$ and $\langle J \rangle$ converge to their respective minima 0 and 0.5. The achieved rates for teh decrease of the expectation values are $\Gamma_v = 0.76\,\mathrm{Hz}$ and $\Gamma_J = 0.49\,\mathrm{Hz}$.

## 7 Conclusions and outlook

We have extensively discussed a scheme which allows to cool simultaneously the internal and external motion of molecules. In particular, we have detailed the rate equations at the basis of the simulations and the *ab initio* calculations of the molecular properties. Special care was taken to use a realistic set of parameters. For these parameters, cooling of the external motion from 1 K to a few $\mu$K can be accomplished in about a second, thus requiring the support of trapping technologies which are stable over these times [10,19,20,51,52,53]. We performed extensive calculations on the OH radical, and studied the cooling efficiency on the molecular properties by comparing the cooling efficiency of OH with the one of NO. We see that, even if NO has more populated rotational levels than OH at the same initial temperature, NO can be cooled faster because of its higher polarizability. We notice that two properties of the polarizability play a different role in the cooling dynamics. In particular, the absolute value of the polarizability is responsible for the processes which cool the rotational excitations, while for vibrational cooling a finite slope of the polarizability as a function of the nuclear coordinate is essential.

An interesting question is how the method performs for more complex molecules. An advantage of larger molecules is that states of even and odd $J$ can be coupled by Raman processes, contrary to the case of linear molecules such as OH and NO. On the other hand, with increasing complexity, the heating due to spontaneous Raman scattering will become more important and must be compensated by a faster coupling to the environment with the help of a better cavity. Additionally, the cooling process can be improved by optimizing the cooling sequence, a task which becomes increasingly difficult with more complex molecules and might require advanced optimization strategies like genetic algorithms [54]. Alternatively, our technique could be extended by combining vacuum-stimulated emission into the cavity with suitably designed Raman pulses using optimal control techniques [23].

*Acknowledgements* G.M. acknowledges the hospitality of the Theoretical Femtochemistry Group at LMU. Support by the European Commission (CONQUEST, MRTN-CT-2003-505089; EMALI, MRTN-CT-2006-035369), the Spanish MEC (Ramon-y-Cajal; Consolider Ingenio 2010 "QOIT"; HA2005-0001), EUROQUAM (Cavity-Mediated Molecular Cooling) and the Deutsche Forschungsgemeinschaft through the excellence cluster "Munich Centre for Advanced Photonics", is acknowledged.

## References

1. G. Morigi, P.W.H. Pinkse, M. Kowalewski and R. de Vivie-Riedle, Phys. Rev. Lett. accepted for publication, arXiv:quant-ph/0703157v2 (2007)
2. see J. Doyle, B. Friedrich, R.V. Krems, F. Masnou-Seeuws, Eur. Phys. J. D. **31**, 149 (2004), and references therein.
3. R.V. Krems, Int. Rev. Phys. Chem. **24**, 99 (2005)
4. Ch. Daussy, T. Marrel, A. Amy-Klein, C.T. Nguyen, Ch.J. Bordé, Ch. Chardonnet, Phys. Rev. Lett. **83**, 1554 (1999)
5. M.R. Tarbutt, H.L. Bethlem, J.J. Hudson, V.L. Ryabov, V.A. Ryzhov, B.E. Sauer, G. Meijer, E.A. Hinds, Phys. Rev. Lett. **92**, 173002 (2004)
6. D. DeMille, Phys. Rev. Lett. **88**, 067901 (2002)
7. C.M. Tesch, R. de Vivie-Riedle, Phys. Rev. Lett. **89**, 157901 (2002)
8. A. André, D. DeMille, J.M. Doyle, M.D. Lukin, S.E. Maxwell, P. Rabl, R.J. Schoelkopf, P. Zoller, Nature Phys. **9**, 636 (2006)
9. D. Kleppner, Phys. Today **57**(8), 12 (2004), and references therein.
10. J.D. Weinstein, R. deCarvalho, T. Guillet, B. Friedrich, J.M. Doyle, Nature (London) **395**, 148 (1998)
11. H.L. Bethlem, G. Berden, G. Meijer, Phys. Rev. Lett. **83**, 1558 (1999)
12. R. Fulton, A.I. Bishop, M.N. Shneider, P.F. Barker, Nature Phys. **2**, 465 (2006)
13. S.A. Rangwala, T. Junglen, T. Rieger, P.W.H. Pinkse, G. Rempe, Phys. Rev. A **67**, 043406 (2003)
14. M.S. Elioff, J.J. Valentini, D.W. Chandler, Science **302**, 1940 (2003)
15. Ning-Ning Liu, H.-J. Loesch Phys. Rev. Lett. **98**, 103002 (2007)
16. C. Cohen-Tannoudji, Rev. Mod. Phys. **70**, 707 (1998)
17. S. Chu, Rev. Mod. Phys. **70**, 685 (1998)
18. W.D. Phillips, Rev. Mod. Phys. **70**, 721 (1998)
19. M. Drewsen, A. Mortensen, R. Martinussen, P. Staanum, J.L. Sørensen, Phys. Rev. Lett. **93**, 243201 (2004)
20. P. Blythe, B. Roth, U. Fröhlich, H. Wenz, S. Schiller, Phys. Rev. Lett. **95**, 183002 (2005)
21. J.T. Bahns, W.C. Stwalley, P.L. Gould, J. Chem. Phys. **104**, 9689 (1996)
22. I.S. Vogelius, L.B. Madsen, M. Drewsen, Phys. Rev. A **70**, 053412 (2004)

23. D.J. Tannor, A. Bartana, J. Phys. Chem, **103**, 10359 (1999)
24. P.W. Brumer, M. Shapiro, Principles of Quantum Control of Molecular processes, (Wiley VCH ed., New York, 2003)
25. P. Horak, G. Hechenblaikner, K.M. Gheri, H. Stecher, H. Ritsch, Phys. Rev. Lett. **79**, 4974 (1997)
26. V. Vuletić, S. Chu, Phys. Rev. Lett. **84**, 3787 (2000)
27. B.L. Lev, A. Vukics, E. R. Hudson, B. C. Sawyer, P. Domokos, H. Ritsch, J. Ye, arXiv:0705.3639v1 (2007)
28. Weiping Lu, Yongkai Zhao, P.F. Barker, Phys. Rev. A 76, 013417 (2007)
29. P. Maunz, T. Puppe, I. Schuster, N. Syassen, P.W.H. Pinkse, G. Rempe, Nature (London) **428**, 50 (2004)
30. S. Nußmann, K. Murr, M. Hijlkema, B. Weber, A. Kuhn, G. Rempe, Nature Phys. **1**, 122 (2005)
31. H.W. Chan, A.T. Black, V. Vuletic, Phys. Rev. Let. **90** 063003 (2003)
32. P. Domokos, H. Ritsch, J. Opt. Soc. Am. B **20**, 1098 (2003)
33. S. Stenholm, Rev. Mod. Phys. **58**, 699 (1986)
34. S.Y.T. van de Meerakker, P.H.M. Smeets, N. Vanhaecke, R.T. Jongma, G. Meijer: Phys. Rev. Lett. **94**, 023004 (2005)
35. J.R. Bochinski, E.R. Hudson, H.J. Lewandowski, J. Ye, Phys. Rev. A **70**, 043410 (2004)
36. R. Fulton, A.I. Bishop, M.N. Shneider, P.F. Barker, Nat. Phys. **2**, 465 (2006)
37. K.P. Huber, G. Herzberg, *Molecular Spectra and Molecular Structure - IV. Constants of Diatomic Molecules*, (New York, 1977)
38. G. Placzek, E. Teller, Z. f. Phys. **81**, 209 (1933)
39. R. Gaufres, S. Sportouch, J. Mol. Spec. **39**, 527 (1971)
40. MOLPRO, version 2006.1, a package of ab initio programs, H.-J. Werner, P.J. Knowles, R. Lindh, F.R. Manby, M. Schütz, and others, see http://www.molpro.net.
41. T.H. Dunning Jr., J. Chem. Phys. **90**, 1007 (1989)
42. J. Olsen, P. Jørgensen, J. Chem. Phys. **82**, 3235 (1985)
43. P. Jørgensen, H.J.Aa. Jensen, J. Olsen, J. Chem. Phys. **89**, 3654 (1988)
44. DALTON, a molecular electronic structure program, Release 2.0 (2005), see http://www.kjemi.uio.no/software/dalton/dalton.html
45. W. L. Meerts, A. Dymanus, Chem. Phys. Lett. **23**, 45 (1973)
46. J.E. Rice, R.D. Amos, S.M. Colwell, N.C. Handy, J. Sanz, J. Chem. Phys. **93**, 8828 (1990)
47. D.E. Woon, T.H. Dunning, J. Chem. Phys. **98**, 1358 (1993)
48. W.J. Hehre, R. Ditchfield, J.A. Pople, J. Chem. Phys. **56**, 2257 (1972)
49. B.W. Shore, *The Theory of Coherent Atomic Excitation, 2*, (Wiley-Interscience, New York, 1990)
50. K. Sundermann, R. de Vivie-Riedle, J. Chem. Phys. **110**, 1896 (1999)
51. H.L. Bethlem, G. Berden, F.M.H. Crompvoets, R.T. Jongma, A.J.A. van Roij, G. Meijer, Nature (London) **406**, 491 (2000)
52. T. Rieger, T. Junglen, S.A. Rangwala, P.W.H. Pinkse, G. Rempe, Phys. Rev. Lett. **95**, 173002 (2005)
53. D. DeMille, D.R. Glenn, J. Petricka, Eur. Phys. J. D **31**, 375 (2004)
54. D.E. Goldberg, *Genetic Algorithms in Search, Optimization, and Machine Learning* (Addison-Wesley, Reading, 1997)